Molecular Therapy
Nucleic Acids
Original Article

Ligand-modified rAAV6 vectors with nanoblades allow high-level gene knockin in HSPCs without compromising cell survival

Alejandra Gutierrez-Guerrero,[1,8] Séverine Périan,[1,8] Aurélien Leray,[2,8] Chiara Martinello,[3] Maria Jimena Abrey Recalde,[1] Caroline Costa,[1] Cecilia Iglesias Herrero,[4] Mohammed Bouzelha,[5] Dimitri Alvarez-Dorta,[5] Sébastien G. Gouin,[2] Eduard Ayuso,[6] Oumeya Adjali,[6] Hildegard Büning,[7] David Deniaud,[2] Mathieu Mével,[6] and Els Verhoeyen[1,3]

[1]CIRI – International Center for Infectiology Research, Inserm, U1111, Université Claude Bernard Lyon 1, CNRS, UMR5308, Ecole Normale Supérieure de Lyon, Université Lyon, 69007 Lyon, France; [2]Nantes Université, CNRS, CEISAM UMR 6230, 44000 Nantes, France; [3]Université Côte d'Azur, INSERM, C3M, 06204 Nice, France; [4]Department of Pharmaceutical and Pharmacological Sciences, Laboratory of Molecular Virology and Gene Therapy, KU Leuven, 3000 Leuven, Belgium; [5]Capacités, 16 rue des marchandises, 44200 Nantes, France; [6]Nantes Université, TaRGeT, Translational Research for gene Therapies, CHU de Nantes, INSERM UMR 1089, 44200 Nantes, France; [7]Laboratory for Infection Biology and Gene Transfer, Institute of Experimental Hematology, Hannover Medical School, 30625 Hannover, Germany

Nanoblades are viral particles loaded with the Cas9 protein complexed with gRNA, which allowed efficient gene editing in hematopoietic stem and progenitor cells (HSPCs). Combined with recombinant adeno-associated vector (rAAV) 6 containing two homologous arms to a gene locus resulted in 50% of expression cassette knockin into HSPCs. However, high effective doses of rAAV6 induced HSPC cell death. Here, we demonstrated that, at high doses, rAAV2 was much less toxic for template DNA delivery and allowed transduction levels in HSPCs equivalent to rAAV6. To improve donor template delivery, rAAV2 and rAAV6 were chemically bio-conjugated with a mannose ligand, via the lysine or tyrosine amino acid residues exposed at the adeno-associated vector (AAV) capsid surface. High-level transduction of HSPCs with mannose-coupled rAAV6 vectors accompanied by a remarkable lower toxicity was achieved as compared to control rAAV6 in correlation with highly reduced p53 pathway activation. Mannose-conjugated rAAV6 combined with nanoblades allowed efficient gene knockin and increased survival of HSPCs from 10% to 80% as compared to the unmodified rAAV6 even in the most immature CD34$^+$CD38lowCD90$^+$ hematopoietic stem cell (HSC) population. Summarizing, mannose-conjugated rAAV6 maintained high-level donor mediated gene knockin when combined with nanoblades without inducing significant toxicity for the HSPCs, an important feature for clinical translation of HSPC gene-editing strategies.

INTRODUCTION

Gene addition using lentiviral vectors has found its way to the clinic with great success for the cure of monogenetic blood diseases. However, the risk of genotoxicity remains problematic due to the semi-random integration of these vectors.[1–3] Gene editing is a gene therapy strategy in the ascendency because it can correct the hematopoietic stem and progenitor cell (HSPC) genome with great precision, which will transfer the correction to all derived blood lineages. Gene editing introduces double-strand breaks (DSBs) in a precise locus.[4] One of the most common platforms used today to introduce DSBs is the CRISPR-Cas9 system, which relies on a Cas9 endonuclease that uses a single-guide RNA (sgRNA) sequence to direct the Cas9 to a specific genomic sequence. It can be introduced into primary cells including CD34$^+$ HSPCs by electroporation of ribonucleoproteins (RNPs), a complex of Cas9 protein associated with the sgRNA. The DSB can be repaired by non-homologous end-joining (NHEJ), which often leads to a small sequence deletion or insertion into the target gene and to gene invalidation (gene knockout)[5,6] or to restauration of the translational frame of the gene and thus the missing protein.[7] Moreover, by additionally providing a template for homologous directed recombination (HDR), one can insert a cDNA of a transgene into its endogenous locus, putting it under the control of the endogenous promoter and regulatory elements and thus mediating gene repair. This template can be provided by single-stranded oligonucleotides to correct single mutations or small deletions in a gene.[8] However, for larger donor DNA templates, other delivery systems are required, such as adeno-associated vector (AAV)[9,10] or integration-deficient lentiviral vectors (IDLVs[11,12]). Several reports pointed to recombinant adeno-associated vector 6 (rAAV6) as the best rAAV serotype for template DNA delivery

Received 29 May 2024; accepted 19 February 2025;
https://doi.org/10.1016/j.omtn.2025.102495.

[8]These authors contributed equally

Correspondence: Els Verhoeyen, CIRI – International Center for Infectiology Research, Inserm, U1111, Université Claude Bernard Lyon 1, CNRS, UMR5308, Ecole Normale Supérieure de Lyon, Université Lyon, 69007 Lyon, France.
E-mail: els.verhoeyen@unice.fr

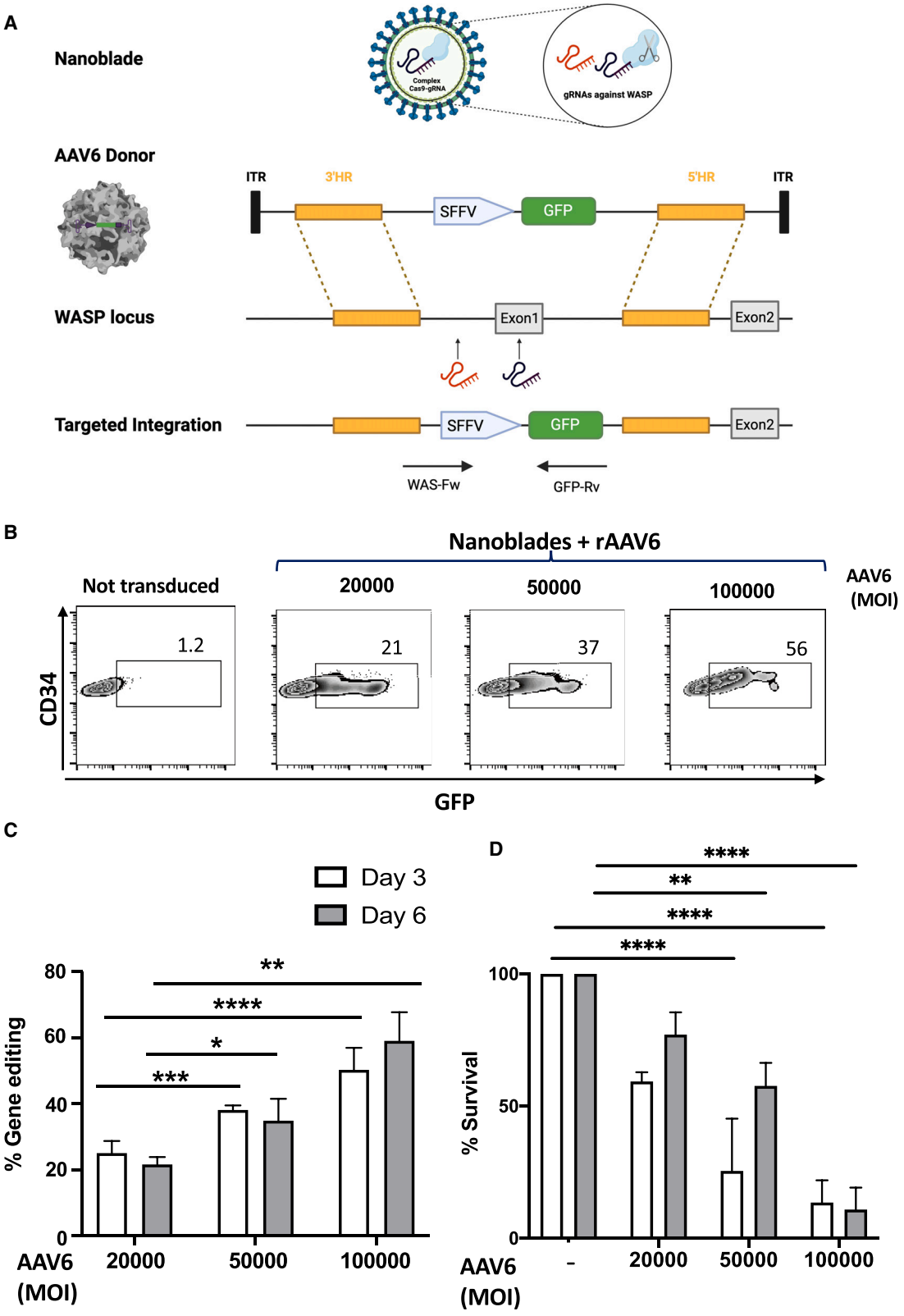

(legend on next page)

into CD34$^+$ HSPCs,[13–15] although rAAV2 has also been suggested to be a good candidate for donor template delivery.[16]

By combining electroporation of CRISPR-Cas9 ribonucleoproteins (RNPs) and rAAV6 for donor template delivery, Pavel-Dinu et al. achieved high levels of targeted gene correction into severe combined immunodeficiency (SCID)-X1 CD34$^+$ HSPCs, which rescued the defect in lymphopoiesis *in vitro* and upon transplantation in NOD/SCIDγC$^{-/-}$ mice.[9,17] The same methodology allowed rAAV6 donor-mediated homologous recombination in the β-globin encoding and *MyD88* loci[18] and also in the pyruvate kinase L/R locus for the treatment of pyruvate kinase deficiency.[10] In addition, genomic loci such as the *IL2RG, AAVS1, and CCR5* genes were modified efficiently using zinc-finger nuclease (ZFN) and an rAAV6 vector encoding for a donor DNA repair template.[19] Even large genome cassettes exceeding the packaging capacity of a single AAV can be split between two rAAV6 donors and precisely integrated into CD34$^+$ cell loci by HDR.[20] However, although high rates of HDR were achieved in CD34$^+$ cells, some toxicity was detected related to rAAV6 since it impaired *in vitro* generation of myeloid colonies and human cell engraftment into immunodeficient mice.[21] We developed a gene-editing delivery system called nanoblades, which are virus like particles derived from murine leukemia virus (MLV) or HIV that can transport the Cas9/gRNA RNPs as cargo and deliver these into human induced pluripotent stem, T, B, and CD34$^+$ cells, resulting in high-level gene editing at specific gene loci.[22,23] More recently, we confirmed that they allowed efficient gene editing of murine and human organoids.[24] Of utmost importance is that the nanoblades did not show any toxicity on these variety of primary cell types. In contrast, the delivery of Cas9/gRNA RNPs by electroporation is accompanied by toxicity and even cell death. In addition, we have shown that combining the nanoblades, which target the Wiskott-Aldrich syndrome (*WAS*) locus, with a donor template delivered by a rAAV6 permitted efficient knockin in HSPCs of up to 50%. Although the nanoblades by themselves did not significantly affect CD34$^+$ cell survival, the rAAV6 encoding for the donor has been reported to be toxic for the CD34$^+$ HSPCs at high doses.[21] In the concern to reduce toxicity of the rAAV6 as donor template, we compared its performance to rAAV2 and to rAAV6 vectors modified at their capsid on lysine or tyrosine residues via conjugation with different amounts of mannose ligands. Interestingly, a balanced quantity of mannose moieties conjugated to the AAV6 capsid combined with nanoblades resulted in efficient knockin in a genomic locus and significantly reduced the toxicity exerted on CD34$^+$ cells as compared to unmodified rAAV6 vector.

RESULTS

Nanoblades combined with rAAV6 delivering a donor DNA result in high-level gene knockin accompanied by high toxicity in human CD34$^+$ cells

Previously, we and others have shown that, for knockin of an expression cassette into a genomic locus, rAAV6s are considered ideal candidates since they allow high-level transduction into CD34$^+$ cells and have been extensively used as vehicles for donor template DNA transfer in combination with CRISPR-Cas9 RNPs.[20,21] We constructed an rAAV6 ssDNA vector genome encoding the sequence for homologous recombination (HR) including 3′ HR and 5′ HR arms of the *WAS* gene at each side of exon 1 (Figure 1A). A GFP reporter cassette under control of the spleen focus-forming virus (SFFV) promoter was inserted between the HR arms. The positions of the gRNAs associating with Cas9 and loaded into the nanoblades as Cas9/WASgRNA RNP complexes are indicated. The resulting targeted integration cassette in *WAS* locus upon HR is represented (Figure 1A). Pre-activated hCD34$^+$ HSPCs were treated with constant quantities of nanoblades and increasing doses of rAAV6 donor template vector. Insertion of the donor template in the *WAS* locus resulted in a significantly higher percentage of GFP$^+$ hCD34$^+$ cells with increasing rAAV6 doses (multiplicity of infection [MOI] 1E5 vector genomes [vg]/cell versus 5E4 vg/cell; Figures 1B and 1C) at day 3 post treatment, which was maintained on day 6 post treatment (Figure 1C), confirming genomic integration of GFP expression cassette by HR. However, it was previously reported that rAAV6 is toxic at higher MOIs in CD34$^+$ cells.[21] As expected, a significant decrease of CD34$^+$ cell survival was detected for nanoblades combined with rAAV6 at MOI 1E5 (10% CD34$^+$ cell survival, day 3), although gene editing was reached up to 50%. Addition of lower doses of rAAV6 donor template vector (MOI 5E4) still induced toxicity (20% CD34$^+$ cell survival, day 3; Figure 1D). A still lower MOI of 2E4 was much less toxic for the CD34$^+$ cells (up to 60% survival). However, this was at cost of CRISPR-Cas9 knockin efficiency (20%) (Figures 1B and 1C).

In summary, an rAAV6 is an efficient vector for introducing the donor template for HDR in combination with nanoblades into CD34$^+$ cells but, at high effective doses, it compromises CD34$^+$ cell survival.

Bio-conjugation of mannose to the lysine or tyrosine residues at the rAAV6 and rAAV2 surface for transduction of CD34$^+$ cells

The rAAV6 functions as an excellent DNA template carrier for CRISPR-Cas9-meditated homology repair in CD34$^+$ cells but at

Figure 1. In combination with nanoblades, rAAV6 allows high-level gene knockin in CD34$^+$ cells but at cost of cell death

(A) Schematic representation of the nanoblades loaded with Cas9 and two sgRNA directed to the *WAS* locus and the rAAV6 genome carrying the donor template DNA for homologous recombination (HR); 3′ HR and 5′ HR arms to the *WAS* gene are indicated. An expression cassette with GFP under control of the SFFV promoter was inserted between these HR arms. Targeted integration into the genomic locus is represented. Drawing was made using BioRender. (B) The FACS analysis of the percentage of gene editing (GFP$^+$ cells) for pre-stimulated CD34$^+$ cells is shown for day 6 post treatment with rAAV6 and a constant amount of nanoblades. MOIs used for rAAV6 are indicated. A summarizing graph of the results for day 3 and day 6 is shown in (C); mean (SD); $n = 4$; four biological repeats using four independent CD34$^+$ cell donors, $^*p < 0.05$, $^{**}p < 0.01$, $^{***}p < 0.001$, $^{****}p < 0.0001$. (D) The percentage of CD34$^+$ cell survival upon incubation with indicated increasing MOIs of rAAV6 by DAPI staining and FACS analysis; mean (SD); $n = 4$; four biological repeats using four independent CD34$^+$ cell donors; one-way ANOVA, Tukey's multiple comparisons test, $^{****}p < 0.0001$, $^{**}p < 0.01$.

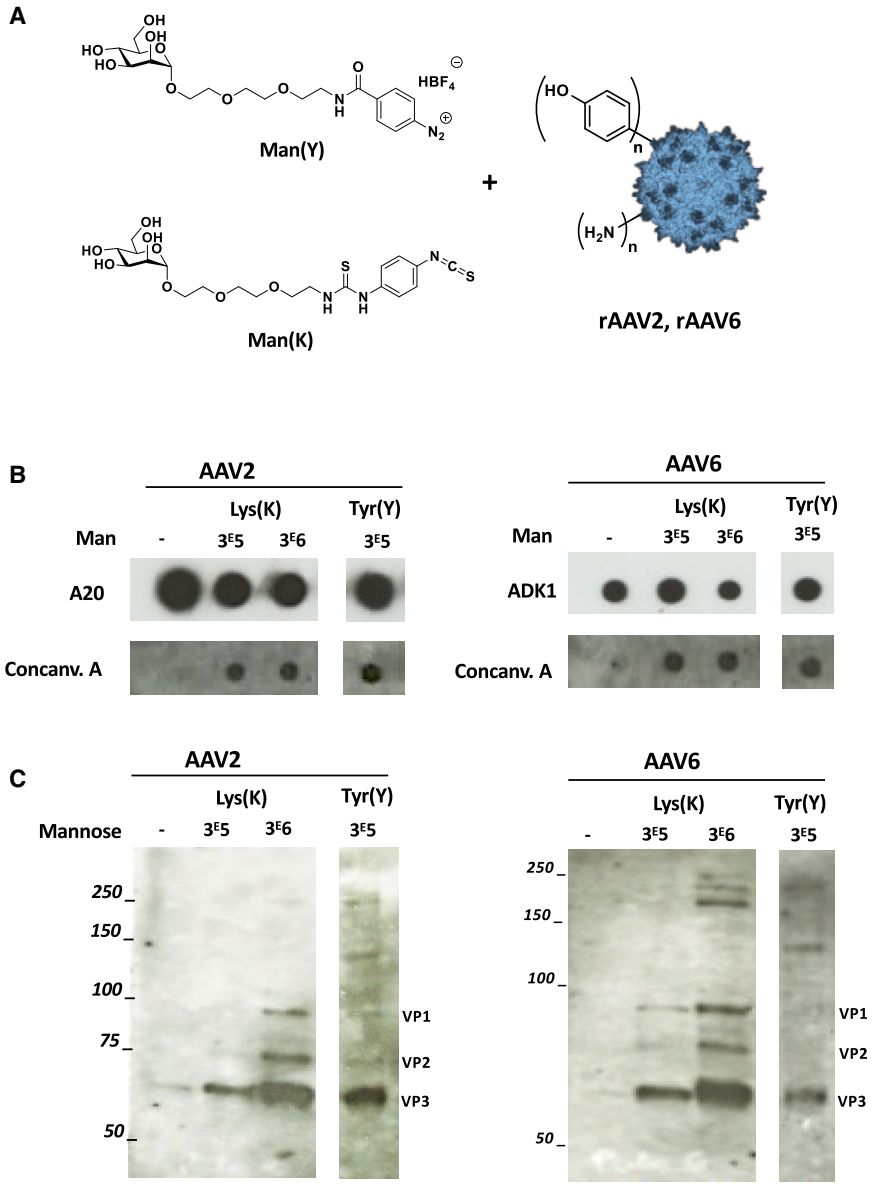

Figure 2. Characterization of rAAV2 and rAAV6 vectors bio-conjugated to mannose via lysine or tyrosine residues

(A) Schematic representation of the bio-conjugation reaction of mannose ligands on lysine or tyrosine residues exposed by the capsids of rAAV2 and rAAV6; 3E5 or 3E6 mannose sugars were incubated for 4 h at RT with 10E12 vg of rAAV2 or rAAV6 vectors encoding for the donor template depicted in Figure 1A. (B) 10E9 vg rAAV vector per condition were analyzed in dot blot using the A20 antibody for AAV2 and the ADK1 antibody for rAAV6, each recognizing the intact assembled capsid of the corresponding AAV. Concanavalin A was employed to detect mannose coupling to the AAV vector particles. Representative of n = 3 biological replicates. (C) 5 × 10E8 vg of rAAV2 or rAAV6 vectors bio-conjugated with mannose at indicated quantities on lysine or tyrosine residues were analyzed by blot for specific presence of mannose by staining with concanavalin A. Representative of n = 3 biological replicates.

cost of cell survival. This high level of toxicity on HSPCs compromises their use in a clinical setting since a minimum number must be infused into a patient to be successful.

With the objective to reduce rAAV6 toxicity on CD34$^+$ cells, we conjugated mannose as a ligand[25] at its surface that might mask certain peptides or epitopes, responsible for binding to the CD34$^+$ cells and inducing cytotoxicity. In parallel, we also bio-conjugated the same mannose moiety to the rAAV2 surface, although it was shown that rAAV2 was less toxic for CD34$^+$ cells than rAAV6.[16]

Previously, we have shown that it is possible to chemically modify some of the amino acids exposed on the surface of AAV vectors.[25] Lysine is a suitable candidate because of the chemical reactivity of its side chain and the abundance at the surface of rAAV of about 480 lysines accessible for chemical reaction on rAAV2 capsid. Another amino acid (aa) that is accessibly exposed at the rAAV surface is tyrosine, with about 320 residues available for bio-conjuction.[26,27] We used both lysine and tyrosine here to introduce a ligand at the rAAV surface by click chemistry (Figure 2A). For lysine bio-conjugation, chemical coupling was achieved through the nucleophilic addition of the amino group of the capsid proteins to the reactive isothiocyanate group of Man(K), resulting in a thiourea bond between the rAAV and the mannose ligand. In contrast, for tyrosine bio-conjugation, aryldiazonium salts Man(Y), generated from the corresponding aniline by reaction with a nitrite in an acidic medium, form a diazo bond with the phenolic side chain of Y on the rAAV capsid via electrophilic aromatic substitution (Figure 2A). We chose the sugar moiety mannose as conjugation partner for surface shielding of rAAV. After chemically coupling different quantities of mannose to the rAAV2 and rAAV6 surface (Table S1) and subsequent purification of the rAAV vectors using dialysis, we evaluated the efficient coupling of mannose to the capsid. We first detected the capsid proteins using a specific antibody (A20 for rAAV2 and ADK1 for rAAV6) that recognized the assembled capsid and confirmed the capsids were intact and not disturbed by the coupling of mannose (Man(K) or Man(Y) as well to rAAV2 as rAAV6; Figure 2B). The specific coupling of mannose to the capsid of rAAV6 and rAAV2 was confirmed by concanavalin A staining for mannose (Figure 2B). We then further characterized the mannose conjugation to the three different capsid VP proteins (VP1, VP2, and VP3) by western blot using concanavalin

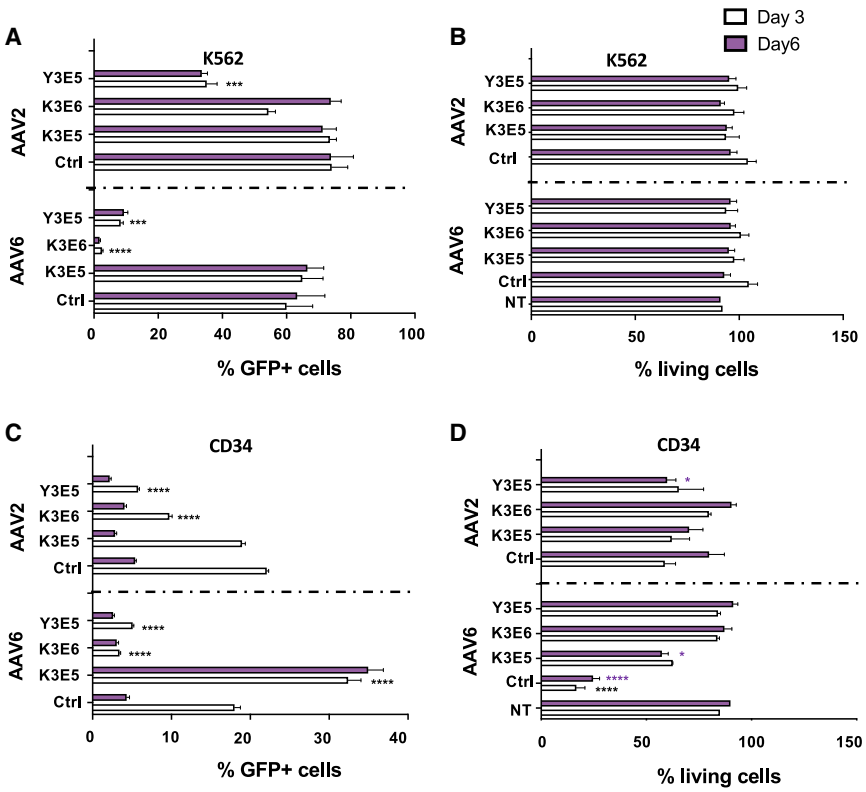

Figure 3. Coupling of rAAV6 with low equivalents of mannose increased transduction of CD34⁺ cells while preventing induction of cell death

(A and B) K562 cells were transduced at an MOI of 50,000 (vg/cell) with the unmodified rAAV2 and rAAV6 vectors (control [Ctrl]) or with rAAV2 and rAAV6 bio-conjugated with mannose sugars at their lysine residues (K3E5 or K3E6) or tyrosine residues (Y3E5; see also Table S1). At day 3 and 6 post transduction, the % of GFP-positive K562 cells (A) and their survival (B) were determined by FACS. Mean (SD); $n = 3$ biological repeats; multiple Student's t test, Tukey's multiple comparisons test, $^{***}p < 0.001$, $^{****}p < 0.001$. (C and D) CD34⁺ cells were pre-stimulated with cytokines overnight and were then transduced at an MOI of 50,000 (vg/cell) with the unmodified rAAV2 and rAAV6 vectors (Ctrl) or with rAAV2 and rAAV6 bio-conjugated with mannose sugars at their lysine residues (K3E5 or K3E6) or tyrosine residues (Y3E5). At day 3 and 6 post transduction, the % of GFP-positive CD34⁺ cells (C) and their survival using DAPI staining (D) was determined by FACS. Mean (SD); $n = 3$; three biological repeats, for which three independent CD34⁺ cell donors were used; multiple Student's t test, Tukey's multiple comparisons test; $^{*}p < 0.05$, $^{****}p < 0.0001$.

A. The VP3 band was more intense for all the conditions since VP3 is incorporated 10 times more than VP1 and VP2 into the capsid regardless of the number of mannose moieties conjugated to the rAAV2 or rAAV6 particles (Figure 2C). The conjugation of mannose to VP1, VP2, and VP3 was only clearly detected in the condition for the highest quantity of sugar conjugated (3E6; Figure 2C). We also confirmed these data by gel separation of purified vector lysate and silver staining, which revealed that the three VP capsid subunits remained intact. A significant augmentation of the molecular mass of the three different VPs was detected when rAAV vectors were bio-conjugated with 3E6 mannose equivalents (Figure S1). Additionally, coupling with 3E5 or 3E6 equivalents of mannose affected slightly as well the rAAV titers (vector genomes/mL), as the infectious titers can likely be attributed to the masking of the rAAV2 and rAAV6 capsid-binding sites by the sugar moieties to their natural receptors (Table S2).

In conclusion, both rAAV6 and rAAV2 showed efficient chemical ligation with mannose as well via their lysine as their tyrosine residues are accessible at the surface of the rAAV capsid.

rAAV6 and rAAV2 allowed efficient transduction of the K562 cells and CD34⁺ cells at low-level bio-conjugation with mannose sugars

Since nanoblades were shown to be not toxic to CD34⁺ cells,[23] we first evaluated in absence of the nanoblades the transduction efficiency as well as the toxicity of rAAV6 and rAAV2 donor template vectors (Figure 1A) bio-conjugated with different amounts of mannose (3E5 and 3E6 equivalents; Table S1) on the K562 hematopoietic cell line and on primary freshly isolated and pre-stimulated CD34⁺ cells. For K562 cells, we detected no reduction in transduction efficiency at MOI 50,000 (% GFP⁺ cells) for rAAV2 and rAAV6 when they were coupled on their lysine residues with 3E5 mannose (K) equivalents as compared to the uncoupled counterparts (Figure 3A). In contrast, transduction of K562 cells was hindered when rAAV6 was bio-conjugated at its lysine residues with 10-fold more mannose moieties (K3E6) or at its tyrosine residues with lower levels of mannose (Y3E5; Figure 3A). For rAAV2 bio-conjugated at its lysine with 10-fold more mannose moieties (K3E6) there was no effect on transduction efficiency compared the control rAAV2. However, similar to rAAV6 bio-conjugated at its tyrosine residues (Y3E5), rAAV2 (Y3E5) transduction was reduced by 2-fold (Figure 3A). No negative effect on K562 cell survival was detected for any of the vectors bio-conjugated with mannose or not as compared to un-transduced cells (Figure 3B). Subsequently, CD34⁺ cells pre-stimulated with early-acting cytokines were transduced with the same panel of rAAV vectors at an MOI of 50,000. First of all, as previously reported, rAAV2 control donor template vector achieved similar transduction efficiencies to rAAV6 control vectors in CD34⁺ cells (Figure 3C and Veldwijk et al. and Schuhmann et al.[13,16]). In contrast to rAAV6, though, unmodified rAAV2 did not reduce CD34⁺ cell survival (Figure 3D). Comparing rAAV6 with its capsid lysine residues conjugated to mannose at low equivalents (K3E5) showed an increased (2-fold) transduction efficiency

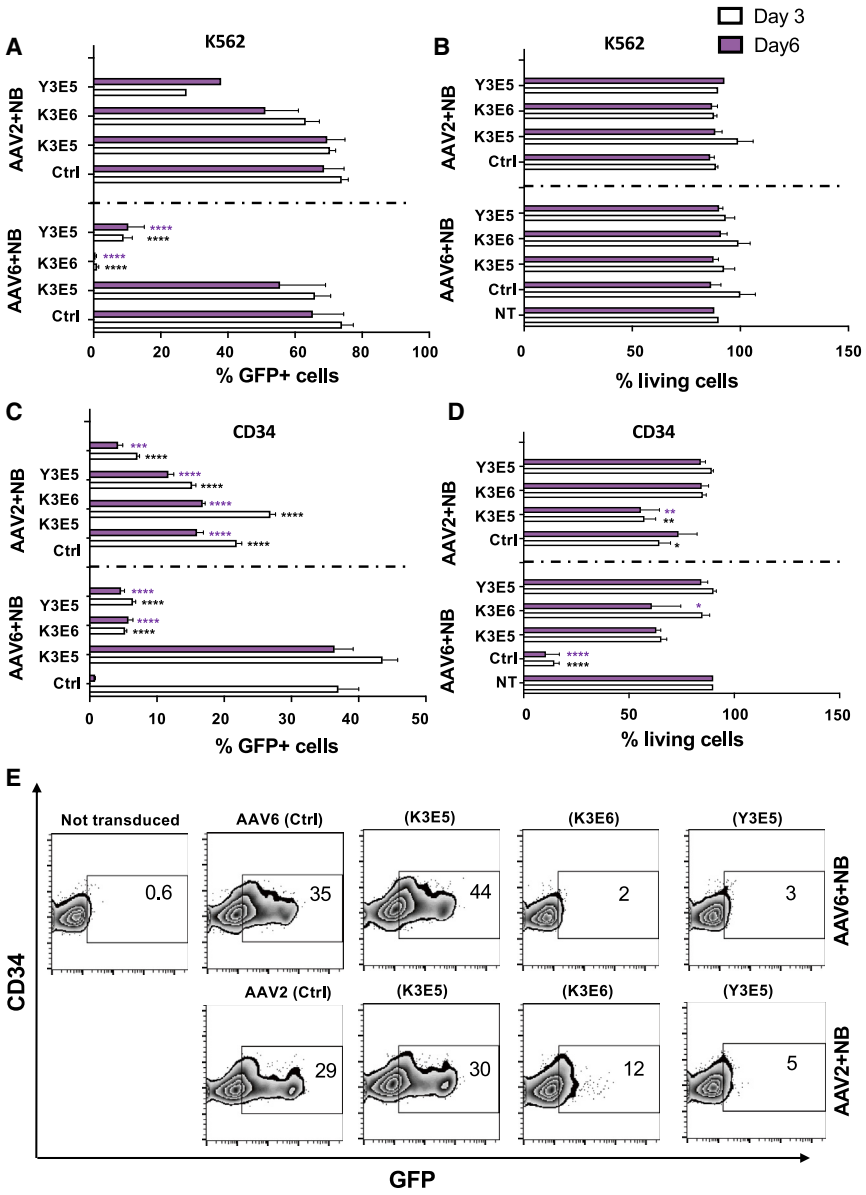

Figure 4. Bio-conjugation of rAAV6 with mannose allowed high-level nanoblade-mediated knockin into CD34$^+$ cells and reduced cell death

(A and B) K562 cells were transduced at an MOI of 50,000 (vg/cell) with the unmodified rAAV2 and rAAV6 vectors (Ctrl) or with rAAV2 and rAAV6 bio-conjugated with mannose sugars at their lysine residues (K3E5 or K3E6) or tyrosine residues (Y3E5) in the presence of nanoblades. At day 3 and 6 post incubation with rAAV vectors and nanoblades, the % of knockin was determined by % of (A) GFP-expressing K562 cells and their survival using DAPI staining (B) analyzed by FACS; mean (SD); $n = 3$; three biological repeats; multiple Student's t test, Tukey's multiple comparisons test; $^{****}p < 0.001$. (C and D) CD34$^+$ cells were pre-stimulated with cytokines overnight and were then transduced at an MOI of 50,000 (vg/cell) with the unmodified rAAV2 and rAAV6 vectors (Ctrl) or with rAAV2 and rAAV6 bio-conjugated with mannose sugars at their lysine residues (K3E5 or K3E6) or tyrosine residues (Y3E5; see also Table S1) in the presence of nanoblades. At day 3 and 6 post transduction, the % of GFP-positive CD34$^+$ cells (% knockin; C) and their survival (D) were determined using FACS analysis; mean (SD); $n = 3$; three biological repeats for which three independent CD34$^+$ cell donors were used; multiple Student's t test, Tukey's multiple comparisons test; $^*p < 0.05$, $^{**}p < 0.01$, $^{***}p < 0.001$, $^{****}p < 0.0001$. (E) Representative FACS analysis for the data in (C) showing gene knockin by analysis of GFP expression in the CD34$^+$ cells at day 6.

compared to unconjugated rAAV6 (Figure 3C). However, rAAV6 (K3E5) significantly augmented CD34$^+$ cell survival from 20% (rAAV6) to over 70% (Figure 3D). If more mannose sugars were ligated to rAAV6 (K3E6), though, transduction efficiency was reduced 5-fold compared to rAAV6 control vector, while CD34$^+$ cell survival was equivalent to untransduced cells. In addition, bio-conjugation of mannose on rAAV6 and rAAV2 tyrosine residues (Y3E5) reduced transduction levels significantly as compared to rAAV6 control vector (Figure 3C). Finally, in the case of rAAV2 bio-conjugated with mannose on lysine residues at low or high quantities (K3E5 or K3E6 equivalents), no improvement in transduction compared to rAAV2 or rAAV6 controls was detected and no negative effect on CD34$^+$ viability was revealed. Of note, all rAAV6 and rAAV2 vectors, capsid modified or not, showed a decrease in GFP$^+$ cells at day 6 post transduction due to the fact that rAAV vectors are largely non-integrating.

Summarizing, rAAV6 conjugated with K3E5 mannose equivalents at its capsid lysine residues showed higher level transduction of CD34$^+$ cells accompanied with a significant reduction of cell death as compared to the unmodified rAAV6 control vector.

rAAV6 and rAAV2 vectors bio-conjugated with low amounts of mannose permitted efficient knockin in CD34$^+$ cells without compromising their survival

The above results indicated strongly that ligation of high levels of mannose moieties (K3E6) on lysine or conjugation of mannose on exposed tyrosine residues (K3E5) on rAAV2 and rAAV6 vectors was deleterious for the transduction efficiency in K562 cells and primary CD34$^+$ cells. We wanted to evaluated whether transduction of K562 cells and pre-stimulated CD34$^+$ cells with mannose-conjugated rAAV6 and rAAV2 donor template vectors in the presence of nanoblades allowed high-level knockin in these cells with reduced toxicity as compared to unmodified rAAV6 (Figures 4 and S2). Indeed, for K562 cells, we detected no significant reduction in

knockin efficiency at MOI 50,000 (% GFP^+ cells) for rAAV2 and rAAV6 when they were coupled on their lysine residues with 3E5 mannose equivalents as compared to the uncoupled counterparts (Figure 4A). In contrast, knockin of the GFP expression cassette in K562 cells was completely hampered when the rAAV6 donor vector was bio-conjugated at its lysine with 10-fold more mannose equivalents (K3E6) and strongly reduced when its tyrosine residues were coupled with lower levels of mannose (YE5; Figure 4A). For rAAV2 bio-conjugated at its lysine with 10-fold more mannose moieties (K3E6), there was no effect on knockin efficiency as compared to the control rAAV2. However, bio-conjugation at its tyrosine residues reduced knockin of rAAV2 donor DNA by 2-fold (Figure 4A). As seen for incubation solely with rAAV2 and rAAV6 vectors, no K562 cell death was detected for any of the vectors bio-conjugated with mannose or not, even in the presence of nanoblades (Figure 4B). Subsequently, pre-stimulated $CD34^+$ cells were transduced with the same panel of rAAV vectors at an MOI of 50,000 but now in the presence of nanoblades. We observed that rAAV2 control donor template vector combined with nanoblades achieved 2-fold lower knockin efficiency in $CD34^+$ cells as compared to rAAV6 control vector in the presence of nanoblades (Figures 4C and 4E). In contrast to rAAV6, though, rAAV2 in presence of nanoblades only slightly reduced $CD34^+$ cell survival (Figure 4D). Comparing rAAV6 conjugated to low equivalents of mannose (K3E5) showed a high-level knockin equivalent to unconjugated rAAV6 in the presence of nanoblades (Figure 4C). Importantly, addition of mannose on the rAAV6 capsid significantly augmented $CD34^+$ cell survival from 10% for control rAAV6 to 70% for K3E5 mannose-coupled rAAV6 when combined with nanoblades (Figure 4D). If more mannose sugars were ligated to rAAV6 (K3E6), though, knockin efficiency was reduced 5-fold as compared to rAAV6 control vector in the presence of nanoblades, while $CD34^+$ cell survival was equivalent to cells that remained untreated. Further bio-conjugation of mannose on rAAV6 and rAAV2 tyrosine residues (Y3E5) combined with nanoblades reduced knockin levels significantly as compared to rAAV6 control vector in the presence of nanoblades (Figures 4C and 4E). Finally, in the case of rAAV2 bio-conjugated with mannose on lysine residues at high or low quantities (K3E5 or K3E6), knockin levels were compromised as compared to rAAV2 or rAAV6 controls when combined with nanoblade (Figure 4C). Viability was only reduced slightly for K3E5 mannose equivalents coupled to rAAV2 and not at all for K3E6 mannose-coupled rAAV2 compared to non-treated $CD34^+$ cells (Figure 4D). Subsequently, we evaluated whether reducing the amount of mannose coupling to lysine residues with K8E4 mannose equivalents or increasing it by using K8E5 mannose equivalents for coupling to rAAV6 would affect knockin levels and survival of $CD34^+$ cells. We first detected the capsid proteins in a dot plot of purified AAV6 vector lysate using the specific ADK1 antibody that recognized the assembled AAV6 capsid and confirmed it was intact (Figure 5A). The specific coupling of mannose to the capsid of rAAV6 and rAAV2 was revealed by concanavalin A staining (Figure 5A). Silver staining showed that the mannosylated VP1, VP2, and VP3 were intact after the chemical coupling (Figure 5B). The pre-stimulated $CD34^+$ cells were transduced with the rAAV6 control vector or rAAV6 coupled at their lysine residues with increasing amounts of mannose (K8E4, K3E5, K8E5) at an MOI of 50,000 in the presence of nanoblades. Compared to uncoupled rAAV6 or rAAV6 conjugated with K3E5 mannose moieties, rAAV6 coupled with K8E4 mannose showed an equivalent level of knockin in $CD34^+$ cells while not significantly affecting $CD34^+$ survival (Figures 5C and 5D). In contrast, augmenting the number of mannose molecules to K8E5 resulted in drastic reduction of knockin in $CD34^+$ cells without cell death induction (Figures 5C and 5D). Interestingly, nanoblades combined with mannose-coupled rAAV6 (K3E5)-mediated knockin detected by GFP revealed a slight bias for the very immature $CD34^+CD38^{low}CD90^+$ stem cell population (Figure 5E).

Summarizing, rAAV6 conjugated with 3E5 mannose equivalents at its capsid's lysine residues combined with nanoblades showed equivalent knockin levels for $CD34^+$ cells accompanied with a significant reduction of cell death as compared to the rAAV6 control vectors.

rAAV6 vectors bio-conjugated with low amounts of mannose permitted efficient knockin in $CD34^+$ cells without toxicity due to reduced p53 response

We then further evaluated toxic side effects by differentiating $CD34^+$ cells treated with nanoblades and rAAV6 coupled with increasing levels of mannose into myeloid lineages. As control, we incubated the $CD34^+$ cells with nanoblades alone, unmodified rAAV6 alone combined with nanoblades, or nanoblades without Cas9 (del Cas9). We determined the number of myeloid colonies at 14 days of culture. A strong reduction in colony numbers was shown in each condition for which rAAV6 without conjugation was present, while the number of colonies increased with increasing amounts of mannose sugars bio-conjugated to the rAAV6 surface (Figure 6A). As expected, stable knockin was detected (% GFP^+ colony forming cell [CFC] colonies) for incubations with nanoblade in presence of unmodified rAAV6, rAAV6 K8E4, and rAAVK8E5, while AAV6 or nanoblade alone resulted in absence of GFP^+ CFCs (Figure 6B). In addition, stable knockin was confirmed by PCR using the *WAS*-forward (Fw) and *GFP*-reverse (Rv) primer pair indicated in Figure 1A performed on genomic DNA of the bulk CFC colonies (Figure 6C).

We demonstrated that ligation of more than 8E5 mannose equivalents on the AAV6 capsid negatively impacts the rAAV6 transduction efficiency of $CD34^+$ cells (Figure 5C). Linking too many mannose molecules on the capsid might indeed prohibit efficient binding to the natural receptors of AAV6 present on $CD34^+$ cells by masking the receptor-binding sites. Interestingly, increasing the mannose equivalents coupled to the rAAV6 surface reduced the negative effect on $CD34^+$ cell survival. One can speculate that hindering entry through the AAV6 receptor by these sugars might reduce the number of AAV genomes entering the cell cytoplasm of $CD34^+$ cells, which consequently reduces the DNA damage

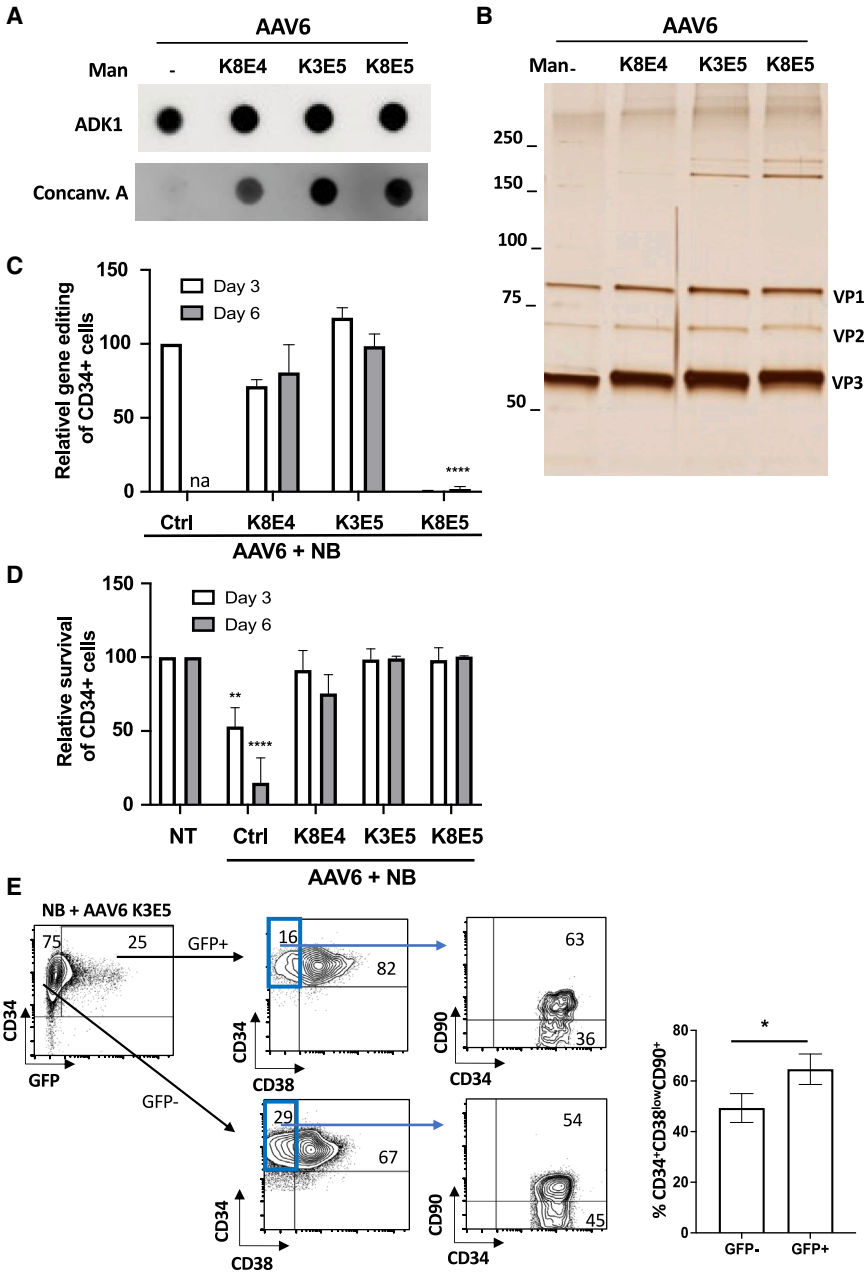

Figure 5. Coupling of rAAV6 with low amounts of mannose allowed high-level nanoblade-mediated knockin CD34⁺ cells without cell death induction

(A) 8E4, 3E5, or 8E5 mannose sugars were incubated for 4 h at RT with 10E12 vg of rAAV6 vectors encoding for the donor template. 10E9 vg rAAV6 vector per condition were analyzed in dot blot using the ADK1 antibody for rAAV6 that recognizes the intact assembled capsid or concanavalin A, which detected mannose bound to the capsid. (B) 5E8 vg of rAAV6 conjugated with indicated quantities of mannose were separated on a gel, followed by silver staining to reveal the intact capsids. (C and D) CD34⁺ cells were pre-stimulated with cytokines overnight and were then transduced at an MOI of 50,000 (vg/cell) with the unmodified rAAV6 vectors (Ctrl) or with rAAV6 bio-conjugated with different quantities of mannose sugars at their lysine residues (K8E4, K3E5, K8E5) in the presence of nanoblades. At day 3 and 6 post transduction, the % of GFP-positive (% knockin) CD34⁺ cells is expressed relative to unmodified rAAV6+NB set to 100% (C) and CD34⁺ cell survival is expressed relative to the untreated cells set to 100% (D) as determined by FACS analysis; mean (SD); $n = 3$; three biological repeats using three independent CD34⁺ cell donors; one-way ANOVA, Tukey's multiple comparisons test; $^{**}p < 0.01$, $^{****}p < 0.0001$. (E) CD34⁺ cells were pre-stimulated with cytokines overnight and were then transduced at an MOI of 50,000 (vg/cell) with rAAV6 bio-conjugated with mannose sugars at their lysine residues (K3E5) in the presence of nanoblades. The very early stem cell population marked by CD34⁺ $CD38^{low}$ CD90⁺ was determined by FACS analysis for the GFP^+ CD34⁺ cells (knockin cells) and GFP^- CD34⁺ cells. The data are summarized in a histogram as mean (SD); $n = 3$; three biological repeats using three independent CD34⁺ cell donors; one-way ANOVA, Tukey's multiple comparisons test; $^{*}p < 0.05$.

response in the cells by triggering a p53-mediated DNA damage response.[28]

We compared untreated, nanoblade-transduced, unmodified rAAV6 (MOI 1E5, 5E4, and 2.5E4), and rAAV6 coupled with K3E5 mannose moieties (MOI 5E4 and 2.5E4) incubated CD34⁺ cells for the level of p53 pathway activation using p21 detection by qPCR. We confirmed that the p53 pathway is strongly activated by unmodified rAAV6 even at the lowest doses used (MOI 2E5 vg/cell), while nanoblade alone and mannose-coupled rAAV6-K3E5 did not trigger this pathway (Figure 6D).

Surface display of mannose moieties on rAAV6 at levels still allowing transduction of CD34⁺ cells reduced the p53 pathway-mediated toxicity as compared to unmodified rAAV6 vectors.

DISCUSSION

Genome editing represents an optimized therapeutic strategy to correct a diseased gene at its endogenous locus and has recently given rise to multiple clinical trials.[29] We demonstrated previously that nanoblades combined with rAAV6 for donor template delivery allow high-level knockin in a specifically targeted genomic locus.[23] However, although nanoblades do not exert any toxicity on the CD34⁺ cells,[23] high doses of rAAV6 required to provide sufficient DNA substrate for HDR severely compromise CD34⁺ HSPC survival. Since a minimum of corrected HSPCs is required for re-infusion into the patients, this toxicity represents a strong drawback for therapeutic applications. Here, we showed that rAAV2 carrying the same donor template represented a valid alternative for rAAV6, allowing high knockin levels while

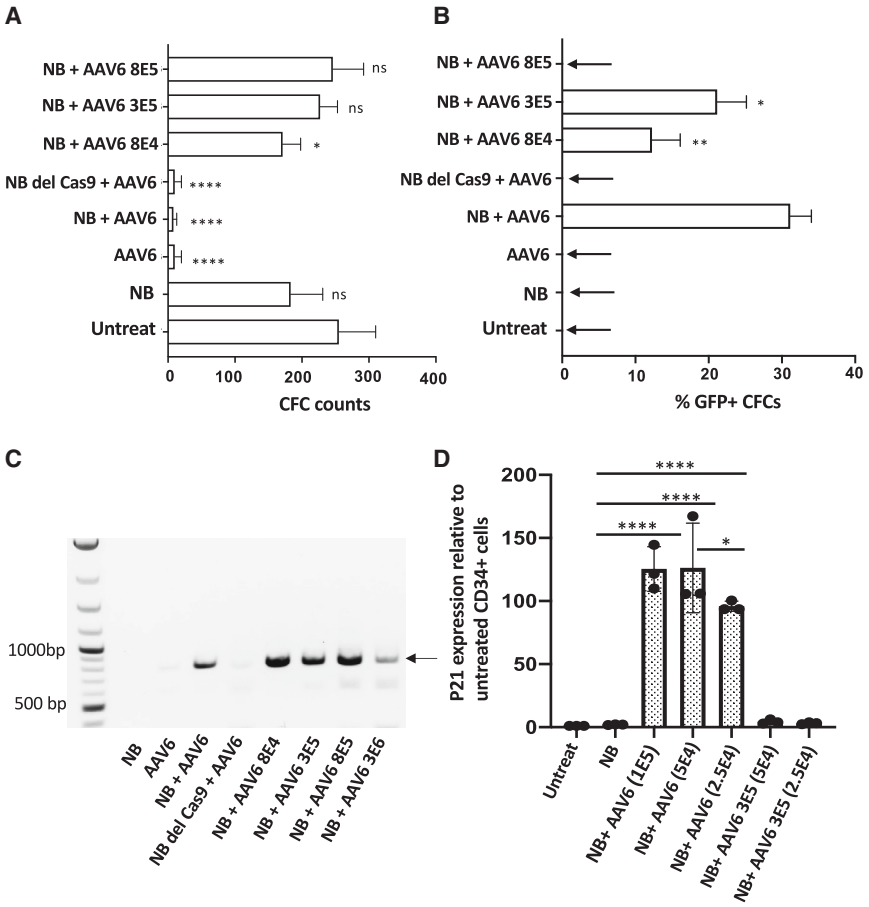

Figure 6. rAAV6 vectors bio-conjugated with mannose do not induce p53 response-mediated toxicity as compared to unmodified rAAV6

(A and B) CD34$^+$ cells were pre-stimulated with cytokines overnight and were then transduced at an MOI of 50,000 (vg/cell) with nanoblade alone, the unmodified rAAV6 vectors, nanoblade without Cas9 (nanoblade del Cas9) combined with rAAV6 vectors, or with rAAV6 bio-conjugated with different quantities of mannose sugars at their lysine residues (K8E4, K3E5, K8E5) in the presence of nanoblades. 500 CD34$^+$ cells were seeded 3 days post transduction in methyl cellulose supplemented with cytokines to induce myeloid differentiation. Two weeks after seeding, the number of colony-forming cells (CFC counts) (A) and the % of GFP$^+$ CFCs (B) was determined; mean (SD); n = 3; three biological repeats using three independent CD34$^+$ cell donors; one-way ANOVA, Tukey's multiple comparisons test; $^*p < 0.05$, $^{***}p < 0.001$, $^{****}p < 0.0001$. (C) Upon isolation of genomic DNA from the CFCs, a PCR was performed using WAS-Fw and GFP-Rv primers (see Figure 1A) to confirm stable knockin. (D) CD34$^+$ cells were pre-stimulated with cytokines overnight and were then left untreated or transduced with nanoblade alone or with rAAV6 (MOI of 1E5, 5E4, 2.5E4 vg/cell) or rAAV6 bio-conjugated with mannose sugars at their lysine residues (K3E5) (MOI of 5E4, 2.5E4 vg/cell) in the presence of nanoblades. At 24 h, CD34$^+$ cells were harvested and the amount of p21 was detected by qPCR. The data are summarized relative to the untransduced cells set to 1; mean (SD); n = 3; three biological repeats using three independent CD34$^+$ cell donors; one-way ANOVA, Tukey's multiple comparisons test; $^*p < 0.05$, $^{****}p < 0.0001$.

preventing CD34$^+$ cell death. Alternatively, by masking the rAAV6 surface through conjugation of lysine residues of the viral capsid with sugars, in this case mannose, nanoblade-mediated knockin yielded CD34$^+$ cell survival similar to CD34$^+$ cells not exposed to rAAV6 vectors. Moreover, mannose bio-conjugated rAAV6 might provide an improved carrier for the HDR template in combination with nanoblades to obtain therapeutically relevant levels of corrected HSPCs for patient treatment.

AAV vectors can easily accommodate homology regions required for HDR-mediated gene correction since their package-limit is 4.7 kb. Additionally, rAAVs are manufactured at high titers for clinical applications, can be stored long term, and are already approved for *in vivo* treatment of various genetic diseases such as hemophilia, spinal muscular atrophies, muscular dystrophies, and retinal blindness, emphasizing their validity as new medicinal products.[30–32] To engineer ligand bio-conjugated rAAVs, one can rely on the standard approved production and purification methods in a first step, followed by a chemical coupling reaction to link sugars or other ligands to these rAAV preparations. No prior genetic modification of the capsid is required, which might impact the rAAV production process and/or titer. Importantly, different AAV serotypes target different tissues according to the presence or not of their entry receptors on the target cell.[33] Although an initial report underlined that AAV2 serotype vectors were not suitable for hCD34$^+$ transduction,[34] this was later rectified by others who showed encouraging transduction levels for rAAV2 into CD34$^+$ cells.[16,35] The discrepancy between these studies might be explained by different doses of rAAV2 used for CD34$^+$ cell transduction. Our data have shown that rAAV2 can be used for delivery of a template for HR into CD34$^+$ cells, although this resulted in a 40% loss of knockin levels as compared to unmodified rAAV6. In return, CD34$^+$ cell survival upon rAAV2 incubation was not compromised as compared to non-treated cells, while rAAV6 was revealed to be very toxic. Different factors might contribute to the toxicity of the rAAV6 on HSPCs. One possibility is that the rAAV genome released in the cells can induce a DNA damage response, which contributes to the decrease in engraftment of gene-edited HSPCs.[28,36,37] This is due to a prolonged persistence of rAAV genomes and their fragments, which trigger a p53-mediated DNA damage response upon recruiting the MRE11-RAD50-NBS1 complex on the rAAV inverted terminal repeats (ITRs). Indeed, interfering with the p53 response by several methods improved survival of gene-editing-corrected HSPCs by blocking the different reactions of cell-cycle arrest,

senescence, and apoptosis.[9,17] Additionally, blocking the p53 pathway might increase the HDR efficiency in cells.[38] However, caution is needed since long-term inhibition of the p53 pathway might be risky and have deleterious effects because it can lead to tumor development. Even if *ex vivo* short-term inhibition of p53 might be acceptable, the better option might be to use mannose-coupled rAAV6 vectors and, as shown here, avoid interference with the p53 pathway activation all together (Figure 6) and, by consequence, its toxic effect on the cells. Interestingly, reducing the dose of unmodified rAAV6 to an MOI of 2E4 still activated the p53 pathway, although there was a tendency to lower p53 activation compared to the higher MOIs (1E5 and 5E4 vg/cell) used, especially when there is no need for a harsh method such as electroporation of the Cas9/gRNA RNPs but we can combine the mannose-bio-conjugated rAAV6 vector with the nanoblades, which do not exert a toxic effect on the HSPCs.[23] Alternatively, it was also shown that replacing rAAV6 by IDLVs for HR template delivery induced lower DNA load and less persistent DNA damage response, improving clonogenic capacity and editing efficiency in long-term repopulating HSPCs.[39]

Wang et al.[19] have shown that homology-driven genome editing in HSPCs was possible using electroporation of zinc finger nuclease (ZFN) mRNA combined with rAAV6 donor delivery. Moreover, they confirmed efficient knockin in the primitive subset of $CD34^+$ HSPCs defined as $CD34^+CD33^+CD90^+$ cells, which are enriched for long-term persisting stem cells, characterized by their persistence in immunodeficient mice. Interestingly, this primitive population was more difficult to edit when an IDLV was used for donor delivery.[12] In agreement with Wang et al.,[19] we detected a slight preference for knockin in the $CD34^+$ $CD38^{low}$ $CD90^+$ cells, a subset of $CD34^+$ cells strongly enriched in hematopoietic stem cells (HSCs). Currently, the chosen method to introduce Cas9/gRNA complexes into $CD34^+$ cells is RNP electroporation, since it avoids persistent Cas9 expression, which might induce immune response against edited cells and off-target editing.[40,41] However, RNP electroporation is accompanied by high levels of toxicity on $CD34^+$ cells.[12,42,43] To optimize gene editing into cells with minimal toxicity, we generated the nanoblades, which borrow the retroviral particle entry path for the introduction of the Cas9/gRNA complex into $CD34^+$ cells without any toxic side effect.[22,23] Therefore, the combinations of the nanoblades with a detoxified rAAV6 via conjugation of its capsid to mannose resulted in high-level knockin of the $CD34^+$ cells, and this not at the expense of cell survival. Indeed, differentiation into myeloid lineage demonstrated an equivalent number of CFCs for untreated and mannose-coupled rAAV6 (K3E5) combined with efficient knockin. To evaluate lymphoid differentiation, we engrafted NOD/SCID γc-/- (NSG) mice with nanoblade-treated $CD34^+$ cells, which were successful in terms of humanization. However, when we isolated $CD34^+$ cells from the BM and T cells from the spleen of these mice, we did not confirm the 30% gene editing that was detected in the initial $CD34^+$ cell population (data not shown). This is not surprising since *WAS* knockout $CD34^+$ cells will not engraft in NSG mice if the knockout is not >90% since they have a selective disadvantage compared to WASP-positive $CD34^+$ cells.[44] Moreover, from clinical trials, it became clear that the *WAS* gene therapy conferred selective proliferative advantage for WASP-expressing T and B cells and probably also HSCs.[45] Since our knockin experiments are performed with a GFP expression cassette, we do not restore the *WAS* gene. Therefore, edited cells will not express a functional WASP and, as *WAS* knockout cells, will have a disadvantage in engraftment potential. One important parameter is the density of the mannose bio-conjugated to the AAV capsid since this might interfere with their transduction efficiency. Here, we demonstrated that ligation of more than 3E6 mannose equivalents on the rAAV6 capsid negatively impacts the rAAV6 transduction efficiency of $CD34^+$ cells. Linking too many mannose molecules on the capsid might indeed prohibit efficient binding to the natural receptors of rAAV6 present on $CD34^+$ cells by masking the receptor binding sites. Interestingly, increasing the mannose equivalents coupled to the rAAV6 surface reduced the negative effect on $CD34^+$ cell survival. Hindering entry through the rAAV6 receptor by these sugars might reduce the number of rAAV genomes entering the cell cytoplasm of $CD34^+$ cells, which consequently reduces the DNA damage response in the cells as shown here (Figure 6D). Reducing the MOI of 1E5 to 2E4 also increased $CD34^+$ cell survival (Figure 1C); however, in contrast to the mannose-modified rAAV6, gene editing was lower (60% versus 20% in Figure 1B). Although lower MOI (2E4) for unmodified rAAV6 might lead to lower AAV genome entry, we only detected a slightly lower activation of p21 as compared to higher MOIs (5E4 and 1E5) (Figure 6D).

Here, we demonstrated that the generation of rAAV6 chemically coupled to mannose at its lysine residues can efficiently deliver the donor template into $CD34^+$ cells for therapeutic gene-editing strategies when combined with Cas9/gRNA RNPs delivered by nanoblades. Both nanoblades and mannose-conjugated rAAV6 components induce no toxicity on the HSPCs. Therefore, this provides an excellent tool for precise therapeutic correction in $CD34^+$ HSPCs.

MATERIALS AND METHODS

Plasmids

To construct the GagMLV-CAS9 fusion, sequential insertions of PCR-amplified fragments in an expression plasmid harboring the human cytomegalovirus (CMV) early promoter, the rabbit β-globin intron, and polyadenylation signals were performed. For the construction of the MA-CA-NC sequence from Friend murine leukemia virus (accession number: M93134), the MA/p12 protease-cleavage site (9 aa) and the FLAG-nls-spCas9 (*Streptococcus pyogenes* Cas9) amplified from pLenti CRISPR were fused and the resulting plasmid was called BiCas9.[22] BaEVRless envelope glycoproteins were previously described.[46] All envelope glycoproteins were expressed in the phCMV-G expression plasmid.[47]

The cassette containing SFFV-GFP DNA flanked by the WASP gene 3′ and 5′ homologous arms was excised from pDonor-SFFV-GFP plasmid by Sbf1/Pac1 digestion, blunted, and cloned into plasmid

vector pAAV-MCS-spA (Stratagene) that was previously digested by Pst1/Mfe1, and restriction sites were blunted. The resulting plasmid pAAV-SFFV-GFP contained the ITR2 sequences flanking the donor DNA cassette.

Cell lines

The HEK293T cells (CRL11268; American Type Culture Collection; Rockville, MD) were maintained in Dulbecco's modified Eagle's medium (DMEM, Invitrogen, Edinburgh, Scotland) supplemented with 10% fetal bovine serum (FBS) (PAA Laboratories, Austria) and penicillin/streptomycin (Gibco, Invitrogen, Auckland, New Zealand). The human erythroleukemic cell line K562 (ATCC, Manassas, VA; CCL-243) and the Raji cell line (ATCC; Manassas, VA; CCL-86) were maintained in RPMI 1640 medium (Gibco-BRL, Middlesex, UK), supplemented with 10% FBS and penicillin/streptomycin.

Nanoblade production

Nanoblade particles were generated by transient transfection of HEK293T cells using the $CaPO_4$ method. For MLV-derived nanoblade production, 3 μg of Cas9-MLV-gag encoding plasmid (BiCas9) was added. For co-pseudotyping of nanoblades with BAEVRLess and VSVG, 2 μg of each envelope encoding plasmid was used. Three micrograms of each plasmid coding for a gRNA (301, agcctcgccagagaagacaa and 305, gatgcttggacgaaaatgct) was added as well as 3 μg of the MLV gag-pol encoding plasmid for MLV-based nanoblade production. Medium was replaced by Optimen supplemented with HEPES (Gibco, Invitrogen, Auckland, New Zealand) and penicillin/streptomycin 18 h post transfection. Nanoblades were harvested 48 h post transfection, centrifuged, and filtered through 0.45 μm. Low-speed concentration of the nanoblades was performed overnight at 3,000 × *g* and 4°C. The concentrated nanoblades were collected the following morning and stored at 4°C.

Cas9 quantification in the nanoblades by ELISA

Recombinant Cas9 (New England Biolabs, USA) was used to generate a standard curve (20 μM, six serial dilutions of 1/2), while the nanoblade supernatants were diluted 1/200 and 1/400. The dilutions were performed in coating buffer (1% Triton) and were then coated onto 96-well-plates by incubation overnight at 4°C. The following day, the wells were incubated with washing buffer (phosphate-buffered saline [PBS]/0.05% Tween) and blocked with PBS/0.05%Tween/3%BSA (Sigma). Subsequently the wells were washed and the primary anti-Cas9 antibody (Cas9-7A9-3A3, 14697P; Cell signaling Technology, USA) was added at 1/1,000 dilution in PBS/3% bovin serum albumine (BSA) and incubated at room temperature (RT) for 1 h while shaking. Before and after 1-h incubation with a secondary anti-mouse horseradish peroxidase (HRP) (F6009-X639F South biotech, USA) diluted 1/10,000 in PBS/3%BSA, a wash step was performed. Finally, the mixed tetramethylbenzidine (TMB) substrate solution containing HRP substrate was added for 20 min (Bethyl, TX, USA). Stop reaction was added in each well and protein was measured at 450 nm in a Multiskan FC (Thermo Scientific).

Production of rAAV2 and rAAV6 vectors

The pAAV-SFFV-GFP contained the ITR2 sequences from AAV serotype 2, flanking the donor DNA cassette, and was used to produce recombinant AAV2/6 and AAV2/2 vectors as described previously.[48] Briefly, HEK293 cells in CellStack-5 chambers (CS5) were transfected with two plasmids (pDG6 containing rep2cap6 sequences and adenoviral helper genes, and the vector plasmid pAAV-SFFV-GFP) by the calcium phosphate precipitation method, and cells were harvested 72 h post transfection by centrifugation. The cell pellet was resuspended in Tris-buffered saline (TBS) buffer, and rAAV particles were extracted by freeze-thaw cycles. Upon centrifugation, the supernatant was polyethylene glycol (PEG) precipitated, then purified by double CsCl density gradient ultracentrifugation and finally formulated in 1× DPBS containing Ca^{2+} and Mg^{2+} through dialysis in Slide-A-Lyzer 10K cassettes (Thermo Scientific, Illkirch, France).

Bio-conjugation of rAAV2 and rAAV6 vectors with mannose

Described in detail elsewhere,[25] rAAV-SFFV-GFP rAAV2 and rAAV6 vectors (1E12 vg, 2.49 nmol) were added to a solution of TBS buffer (pH 9.3) containing 3E5 or 3E6 mannose equivalents for lysine and tyrosine conjugation and were incubated for 4 h at RT. Briefly, For lysine bio-conjugation, chemical coupling was achieved through the nucleophilic addition of the amino group of the capsid proteins to the reactive isothiocyanate group of Man(K), resulting in a thiourea bond between the rAAV and the mannose ligand. In contrast, for tyrosine bio-conjugation, the aryldiazonium salt Man(Y), generated from the corresponding aniline by reaction with a nitrite in an acidic medium, form a diazo bond with the phenolic side chain of Y on the rAAV capsid via electrophilic aromatic substitution. The solutions containing the vectors were then dialyzed against Dulbecco's phosphate buffered saline (DPBS) + 0.001% Pluronic to remove free molecules that were not bound to the rAAV capsid.

Titration of rAAV vector genomes (vg)

A total of 3 μL of rAAV was treated with 20 units of DNase I (Roche #04716728001) at 37°C for 45 min to remove residual DNA in vector samples. After treatment with DNase I, 20 μL of proteinase K (20 mg/mL; MACHEREY-NAGEL # 740506) was added and the mixture incubated at 70°C for 20 min. An extraction column (NucleoSpin RNA Virus) was then used to extract DNA from purified rAAV vectors. Real-time qPCR was performed with a StepOnePlus Real-Time PCR system upgrade (Life Technologies). Sequencing primer (Fw), GGAACCCCTAGTGATGGAGTT; primer (Rv), CGGC CTCAGTGAGCGA; and probe, CACTCCCTCTCTGCGCGCTCG were used. All PCRs were performed with a final volume of 20 μL, including primers and probes targeting the ITR2 sequence, PCR Master Mix (TaKaRa), and 5 μL of template DNA (plasmid standard or sample DNA). qPCR was carried out with an initial denaturation step at 95°C for 20 s followed by 45 cycles of denaturation at 95°C for 1 s and annealing/extension at 56°C for 20 s. Plasmid standards were generated with seven serial dilutions (containing 10^8–10^2 plasmid copies), as described by D'Costa et al.[49]

Western blot and silver staining

All vectors were denatured at 100°C for 5 min using Laemmli sample buffer and separated by SDS-PAGE on 10% Tris-glycine polyacrylamide gels (Life Technologies). Precision Plus Protein All Blue Standards (Bio-Rad) were used as a molecular weight size marker. After electrophoresis, gels were either silver stained (PlusOne Silver Staining Kit, Protein; GE Healthcare) or transferred onto nitrocellulose membranes for western blot. After transferring the proteins to nitrocellulose membrane using a transfer buffer (25 mM Tris/192 mM glycine/0.1 [w/v] SDS/20% MeOH) for 1 h at 150 mA in a Trans-Blot SD Semi-Dry Transfer Cell (Bio-Rad), the membrane was saturated for 2 h at RT with 5% semi-skimmed milk in PBS-Tween (0.1%) or with 1% gelatin, 0.1% Igepal in PBS-Tween (0.01%). After saturation, the membrane was probed with the corresponding antibody (anti-capsid polyclonal, B1 monoclonal, or anti-fluorescein-alkaline phosphatase [AP]) and fluorescein isothiocyanate (FITC)-concanavalin A lectin (mannose detection) overnight at 4°C. Three washes (15 min at RT) with PBS-Tween (0.1%) were performed between each stage to remove unbound reagents. Bands were visualized by chemiluminescence using AP or HRP-conjugated secondary antibodies and captured on X-ray film.

Immuno dot-blot analysis

rAAV vectors were loaded at a dose of 10^{10} vg on a nitrocellulose paper soaked briefly in PBS prior to assembling the dot-blot manifold (Bio-Rad). Nitrocellulose membrane containing the vectors was treated as for western blotting.

rAAV infectious titer measurement

The infectivity of each sample was measured as follows. HeLa cells were seeded in 2 mL of DMEM growth medium in six-well culture plates at a density of 10^6 cells/well. Cells were then incubated overnight at 37°C to reach 50% confluence. The vector stock was then diluted 10-fold by serial dilution. Next, 2 μL of each dilution was added to separate wells in the six-well plates. Plates were then incubated at 37°C for 24 h. The infectivity of the rAAV2-SFFV-GFP or rAAV6-SFFV-GFP control were measured immediately upon thawing of the sample. The same procedure was used for mannose bio-conjugated AAV vectors. rAAV-SFFV-GFP-transduced cells were detected by fluorescence microscopy. GFP-fluorescent HeLa cells were manually counted using a fluorescence microscope by three different operators. All the GFP^+ cells obtained after infection of rAAV vector using serial dilutions were counted in three wells of a six-well plate per vector.

The transducing unit (TU) titer was calculated using the following formula:

$TU/mL = (4040 \times NGFP \times dilutions \times 1{,}000)/V$, where NGFP is the mean number of GFP-positive cells per well and V is the volume (in microliters) of vector used to infect cells.

$CD34^+$ cell isolation

Umbilical cord blood (CB) samples from full-term pregnancies (provided by Lyon Sud Hospital, Lyon) were collected in bags containing anticoagulant after informed consent of donors and approval was obtained by the ethics committees of the hospitals according to the Helsinki Declaration. Low-density cells were separated by Ficoll gradient (Sigma-Aldrich, St Louis, MO). $CD34^+$ purification was performed by positive magnetic cell separation using the Automacs pro-separator (Miltenyi Biotech) after staining of the cells with the human $CD34^+$ MicroBead Kit (Miltenyi Biotec). Purity of the selected $CD34^+$ cell fraction was evaluated by fluorescence-activated cell sorting (FACS) analysis (FACSCanto, BD) with APC-conjugated anti-CD34 antibody (Miltenyi Biotech). Cells were frozen in FCS 10% DMSO for later use.

Transduction of cells with nanoblades

For nanoblade transduction into cell lines, 2E5 K562 cells were plated in six- (293T) or 24-well plates (K562, Raji) and nanoblades, equivalent to 4 μmol of Cas9 protein, were added. Cells were pelleted 48 h post transduction for subsequent DNA extraction and PCR. For nanoblade transduction of $CD34^+$ HSPCs, $CD34^+$ cells were thawed and seeded in Cellgro medium (Cell genix, Germany) and stimulated with cytokines (human thrombopoietin [hTPO], 20 ng/mL; human stem cell factor [hSCF], 100 ng/mL; human FMS-like tyrosine kinase 3 ligand [hFlt3-L],100 ng/mL) for 24 h before incubation with nanoblades. Viability was determined before and after nanoblade incubation (see below).

Viability

Viability of $CD34^+$ cells upon nanoblade incubation was determined using Annexin V/propidium iodide staining and was then analyzed by flow cytometry.

K562 and human $CD34^+$ cell treatment with nanoblades and rAAV and evaluation of gene editing

K562 cells and $CD34^+$ cells were treated with nanoblades as described above. Together with the nanoblades, the rAAV6 or rAAV2 vectors delivering the donor cassette were added to the cells at indicated MOIs. $CD34^+$ cells were pre-stimulated 16 h in Cellgro medium supplemented with cytokines (hTPO, 20 ng/mL; hSCF, 100 ng/mL; hFlt3-L; 100 ng/mL) and seeded on plates coated with RetroNectin (Clontech/Takara; 12 μg/mL PBS) according to manufacturer's recommendations prior to nanoblade (4 μmol of Cas9 protein) and rAAV6 addition. Eight hours later, the medium was changed for Cellgro medium supplemented with cytokines and cultured for 48 h. To quantify the gene-editing efficiency, cells were washed, counted, and used for flow cytometry analysis at day 3 and day 6 to confirm stable integration of the donor cassette by the percentage GFP expression. Furthermore, $CD34^+$ cells were seeded in MethoCult H4434 Classic medium, which is already supplemented with rhSCF, rhGM-CSF, rhIL-3, and rhEPO (STEMCELL Technologies) to perform a CFC assay according manufacturer's recommendation and Lévy et al.[50] Numbers of CFCs were determined at day 14 of culture to evaluate toxicity of the combined rAAV6 and nanoblade treatment.

Analysis of stable integration of donor cassette in $CD34^+$ cells and CFCs

Genomic DNA isolated from bulk CFCs was subjected to PCR with one Fw primer situated in the endogenous *WAS* locus, WAS-Fw

(AGGGGCTCGCTCTGTAATTA) and a Rv primer in the reporter GFP, REV-GFP (AACTTGTGGCCGTTTACGTC).

Gene expression analyses

Total RNA was extracted using RNeasy Plus Micro Kit (QIAGEN), according to the manufacturer's instructions, and DNase treatment was performed using RNase-free DNase Set (QIAGEN). Complementary DNA was synthesized with SuperScript VILO IV cDNA Syn-thesis Kit (Thermo Fisher) with DNase treatment. cDNA was then used for qPCR in a Viia7 real-time PCR thermal cycler using TaqMan Gene Expression Assays (Applied Biosystems) to detect the expression of p21 (primers Fw, GGGGCGGTT GTATATCAGG and Rv, GGCTCCACAAGGAACTGACT). As reference the gene encoding *β-actin* was used (primers Fw, TCC GTG TGG ATC GGC GGC TCC A and Rv, CTG CTT GCT GAT CCA CAT CTG). Data were analyzed with QuantStudio Real-Time PCR software v.1.1 (Applied Biosystem). The cycle threshold (Ct) value considered for each sample was calculated as mean of the two/three technical replicates performed. Relative expression of each target gene (Ct) was first normalized to β-actin and then represented as fold changes of the DDCt relative to the untreated sample.

Statistical analysis

All graphs represent the mean (SD). t test was used for two-group comparison. A p value <0.05 was considered to indicate statistical significance. One-way ANOVA followed by Tukey's multiple comparisons test was used for multi-group comparison if the data obeyed the normal distribution. In the case that the data did not obey the normal distribution, Mann-Whitney test was used for two-group comparison and Kruskal-Wallis test was used for multi-group comparison. The statistical tests applied, and p values and number of biological repeats are indicated in the figure legends. Statistical analysis was conducted using Microsoft Excel 2013 and Prism software v6.0 (GraphPad Software, La Jolla, CA, USA).

DATA AVAILABILITY

All data supporting the conclusions of this article are available from the corresponding author upon request.

ACKNOWLEDGMENTS

The authors thank the ViVeM center of TaRGeT, UMR 1089 (INSERM and Nantes Université, which is a bioproduction and biotherapy national integrator (ANR-22-AIBB-0001; http://umr1089.univ-nantes.fr) for the production of the rAAV vectors used in this study. This work was funded by LabEx Ecofect (ANR-11-LABX-0048) of the Université de Lyon, within the program Investissements d'Avenir (ANR-11-IDEX-0007) operated by the French National Research Agency (ANR). This study was supported by research funding (CRISPR screen Action) from the Canceropôle Provence-Alpes-Côte d'Azur. Additionally, funding was received from the CHEMAAV-ANR-19-CE18-0001 grant and the European Joint Program Rare Diseases FANC-EDIT operated by the ANR. This work was funded via the program "Biotherapy and bioproduction of innovative therapies: PEPR-EDITO" by the French government. C.M. is supported by a MARIE SKŁODOWSKA-CURIE ACTIONS PhD network GET-IN and the European Community. We acknowledge the contribution of AniRA lentivectors production facility from the CELPHEDIA Infrastructure and SFR Biosciences (UAR3444/CNRS, US8/Inserm, ENS de Lyon, UCBL).

AUTHOR CONTRIBUTIONS

A.G.-G., A.L., and S.P. were responsible for experimental design, methodology and performing experiments, analysis, and preparation of the figures for the manuscript. C.M., M.J.A.R., C.C., M.B., D.A.-D., C.I.H., and S.G.G. were responsible for performing and analyzing experiments. E.A., H.B., and D.D. were involved in the generation and characterization of mannose-coupled rAAV vectors. E.A., O.A., and H.B. provided advice and reviewed the manuscript. D.D., M.M., and E.V. designed the project, supervised the work, and discussed and analyzed results. E.V. wrote the manuscript.

DECLARATION OF INTERESTS

E.V. is inventor on the patent on pseudotyping of retroviral particles with BaEV envelope glycoproteins (patent WO 07290918.7), which were used here for the nanoblade production.

M.M., D.D., and E.A. are inventors on two patents including the AAV bio-conjugation technology described in this manuscript.

SUPPLEMENTAL INFORMATION

Supplemental information can be found online at https://doi.org/10.1016/j.omtn.2025.102495.

REFERENCES

1. Bougnères, P., Hacein-Bey-Abina, S., Labik, I., Adamsbaum, C., Castaignède, C., Bellesme, C., and Schmidt, M. (2021). Long-Term Follow-Up of Hematopoietic Stem-Cell Gene Therapy for Cerebral Adrenoleukodystrophy. Hum. Gene Ther. *32*, 1260–1269. https://doi.org/10.1089/hum.2021.053.

2. Marcucci, K.T., Jadlowsky, J.K., Hwang, W.-T., Suhoski-Davis, M., Gonzalez, V.E., Kulikovskaya, I., Gupta, M., Lacey, S.F., Plesa, G., Chew, A., et al. (2018). Retroviral and Lentiviral Safety Analysis of Gene-Modified T Cell Products and Infused HIV and Oncology Patients. Mol. Ther. *26*, 269–279. https://doi.org/10.1016/j.ymthe.2017.10.012.

3. Tucci, F., Galimberti, S., Naldini, L., Valsecchi, M.G., and Aiuti, A. (2022). A systematic review and meta-analysis of gene therapy with hematopoietic stem and progenitor cells for monogenic disorders. Nat. Commun. *13*, 1315. https://doi.org/10.1038/s41467-022-28762-2.

4. Branzei, D., and Foiani, M. (2008). Regulation of DNA repair throughout the cell cycle. Nat. Rev. Mol. Cell Biol. *9*, 297–308. https://doi.org/10.1038/nrm2351.

5. Knipping, F., Newby, G.A., Eide, C.R., McElroy, A.N., Nielsen, S.C., Smith, K., Fang, Y., Cornu, T.I., Costa, C., Gutierrez-Guerrero, A., et al. (2022). Disruption of HIV-1 co-receptors CCR5 and CXCR4 in primary human T cells and hematopoietic stem and progenitor cells using base editing. Mol. Ther. *30*, 130–144. https://doi.org/10.1016/j.ymthe.2021.10.026.

6. Mandal, P.K., Ferreira, L.M.R., Collins, R., Meissner, T.B., Boutwell, C.L., Friesen, M., Vrbanac, V., Garrison, B.S., Stortchevoi, A., Bryder, D., et al. (2014). Efficient Ablation of Genes in Human Hematopoietic Stem and Effector Cells using CRISPR/Cas9. Cell Stem Cell *15*, 643–652. https://doi.org/10.1016/j.stem.2014.10.004.

7. Román-Rodríguez, F.J., Ugalde, L., Álvarez, L., Díez, B., Ramírez, M.J., Risueño, C., Cortón, M., Bogliolo, M., Bernal, S., March, F., et al. (2019). NHEJ-Mediated Repair of CRISPR-Cas9-Induced DNA Breaks Efficiently Corrects Mutations in HSPCs from Patients with Fanconi Anemia. Cell Stem Cell *25*, 607–621.e7. https://doi.org/10.1016/j.stem.2019.08.016.

8. Fañanas-Baquero, S., Morín, M., Fernández, S., Ojeda-Perez, I., Dessy-Rodriguez, M., Giurgiu, M., Bueren, J.A., Moreno-Pelayo, M.A., Segovia, J.C., and Quintana-Bustamante, O. (2023). Specific correction of pyruvate kinase deficiency-causing point mutations by CRISPR/Cas9 and single-stranded oligodeoxynucleotides. Front Genome *5*, 1104666. https://doi.org/10.3389/fgeed.2023.1104666.

9. Pavel-Dinu, M., Wiebking, V., Dejene, B.T., Srifa, W., Mantri, S., Nicolas, C.E., Lee, C., Bao, G., Kildebeck, E.J., Punjya, N., et al. (2019). Gene correction for SCID-X1 in long-term hematopoietic stem cells. Nat. Commun. *10*, 1634. https://doi.org/10.1038/s41467-019-09614-y.

10. Fañanas-Baquero, S., Quintana-Bustamante, O., Dever, D.P., Alberquilla, O., Sanchez-Dominguez, R., Camarena, J., Ojeda-Perez, I., Dessy-Rodriguez, M., Turk,

R., Schubert, M.S., et al. (2021). Clinically relevant gene editing in hematopoietic stem cells for the treatment of pyruvate kinase deficiency. Mol. Ther. Methods Clin. Dev. *22*, 237–248. https://doi.org/10.1016/j.omtm.2021.05.001.

11. Lombardo, A., Genovese, P., Beausejour, C.M., Colleoni, S., Lee, Y.-L., Kim, K.A., Ando, D., Urnov, F.D., Galli, C., Gregory, P.D., et al. (2007). Gene editing in human stem cells using zinc finger nucleases and integrase-defective lentiviral vector delivery. Nat. Biotechnol. *25*, 1298–1306. https://doi.org/10.1038/nbt1353.

12. Genovese, P., Schiroli, G., Escobar, G., Tomaso, T.D., Firrito, C., Calabria, A., Moi, D., Mazzieri, R., Bonini, C., Holmes, M.C., et al. (2014). Targeted genome editing in human repopulating haematopoietic stem cells. Nature *510*, 235–240. https://doi.org/10.1038/nature13420.

13. Veldwijk, M.R., Sellner, L., Stiefelhagen, M., Kleinschmidt, J.A., Laufs, S., Topaly, J., Fruehauf, S., Zeller, W.J., and Wenz, F. (2010). Pseudotyped recombinant adeno-associated viral vectors mediate efficient gene transfer into primary human CD34(+) peripheral blood progenitor cells. Cytotherapy *12*, 107–112. https://doi.org/10.3109/14653240903348293.

14. Song, L., Li, X., Jayandharan, G.R., Wang, Y., Aslanidi, G.V., Ling, C., Zhong, L., Gao, G., Yoder, M.C., Ling, C., et al. (2013). High-efficiency transduction of primary human hematopoietic stem cells and erythroid lineage-restricted expression by optimized AAV6 serotype vectors in vitro and in a murine xenograft model in vivo. PLoS One *8*, e58757. https://doi.org/10.1371/journal.pone.0058757.

15. Brault, J., Liu, T., Liu, S., Lawson, A., Choi, U., Kozhushko, N., Bzhilyanskaya, V., Pavel-Dinu, M., Meis, R.J., Eckhaus, M.A., et al. (2022). CRISPR-Cas9-AAV versus lentivector transduction for genome modification of X-linked severe combined immunodeficiency hematopoietic stem cells. Front. Immunol. *13*, 1067417. https://doi.org/10.3389/fimmu.2022.1067417.

16. Schuhmann, N.K., Pozzoli, O., Sallach, J., Huber, A., Avitabile, D., Perabo, L., Rappl, G., Capogrossi, M.C., Hallek, M., Pesce, M., and Büning, H. (2010). Gene transfer into human cord blood-derived CD34(+) cells by adeno-associated viral vectors. Exp. Hematol. *38*, 707–717. https://doi.org/10.1016/j.exphem.2010.04.016.

17. Schiroli, G., Ferrari, S., Conway, A., Jacob, A., Capo, V., Albano, L., Plati, T., Castiello, M.C., Sanvito, F., Gennery, A.R., et al. (2017). Preclinical modeling highlights the therapeutic potential of hematopoietic stem cell gene editing for correction of SCID-X1. Sci. Transl. Med. *9*, eaan0820. https://doi.org/10.1126/scitranslmed.aan0820.

18. Martin, F., Sánchez-Hernández, S., Gutiérrez-Guerrero, A., Pinedo-Gomez, J., and Benabdellah, K. (2016). Biased and Unbiased Methods for the Detection of Off-Target Cleavage by CRISPR/Cas9: An Overview. Indian J. Manag. Sci. *17*, 1507. https://doi.org/10.3390/ijms17091507.

19. Wang, J., Exline, C.M., DeClercq, J.J., Llewellyn, G.N., Hayward, S.B., Li, P.W.-L., Shivak, D.A., Surosky, R.T., Gregory, P.D., Holmes, M.C., and Cannon, P.M. (2015). Homology-driven genome editing in hematopoietic stem and progenitor cells using ZFN mRNA and AAV6 donors. Nat. Biotechnol. *33*, 1256–1263. https://doi.org/10.1038/nbt.3408.

20. Bak, R.O., and Porteus, M.H. (2017). CRISPR-Mediated Integration of Large Gene Cassettes Using AAV Donor Vectors. Cell Rep. *20*, 750–756. https://doi.org/10.1016/j.celrep.2017.06.064.

21. Romero, Z., Lomova, A., Said, S., Miggelbrink, A., Kuo, C.Y., Campo-Fernandez, B., Hoban, M.D., Masiuk, K.E., Clark, D.N., Long, J., et al. (2019). Editing the Sickle Cell Disease Mutation in Human Hematopoietic Stem Cells: Comparison of Endonucleases and Homologous Donor Templates. Mol. Ther. *27*, 1389–1406. https://doi.org/10.1016/j.ymthe.2019.05.014.

22. Mangeot, P.E., Risson, V., Fusil, F., Marnef, A., Laurent, E., Blin, J., Mournetas, V., Massouridès, E., Sohier, T.J.M., Corbin, A., et al. (2019). Genome editing in primary cells and in vivo using viral-derived Nanoblades loaded with Cas9-sgRNA ribonucleoproteins. Nat. Commun. *10*, 45. https://doi.org/10.1038/s41467-018-07845-z.

23. Gutierrez-Guerrero, A., Abrey Recalde, M.J., Mangeot, P.E., Costa, C., Bernadin, O., Périan, S., Fusil, F., Froment, G., Martinez-Turtos, A., Krug, A., et al. (2021). Baboon Envelope Pseudotyped "Nanoblades" Carrying Cas9/gRNA Complexes Allow Efficient Genome Editing in Human T, B, and CD34+ Cells and Knock-in of AAV6-Encoded Donor DNA in CD34+ Cells. Front. Genome Ed. *3*, 604371. https://doi.org/10.3389/fgeed.2021.604371.

24. Tiroille, V., Krug, A., Bokobza, E., Kahi, M., Bulcaen, M., Ensinck, M.M., Geurts, M.H., Hendriks, D., Vermeulen, F., Larbret, F., et al. (2023). Nanoblades allow high-level genome editing in murine and human organoids. Mol. Ther. Nucleic Acids *33*, 57–74. https://doi.org/10.1016/j.omtn.2023.06.004.

25. Mével, M., Pichard, V., Bouzelha, M., Alvarez-Dorta, D., Lalys, P.-A., Provost, N., Allais, M., Mendes, A., Landagaray, E., Ducloyer, J.-B., et al. (2024). Mannose-coupled AAV2: A second-generation AAV vector for increased retinal gene therapy efficiency. Mol. Ther. Methods Clin. Dev. *32*, 101187. https://doi.org/10.1016/j.omtm.2024.101187.

26. Leray, A., Lalys, P.-A., Varin, J., Bouzelha, M., Bourdon, A., Alvarez-Dorta, D., Pavageau, K., Depienne, S., Marchand, M., Mellet, A., et al. (2024). Novel chemical tyrosine functionalization of adeno-associated virus improves gene transfer efficiency in liver and retina. Biomed. Pharmacother. *171*, 116148. https://doi.org/10.1016/j.biopha.2024.116148.

27. Mével, M., Bouzelha, M., Leray, A., Pacouret, S., Guilbaud, M., Penaud-Budloo, M., Alvarez-Dorta, D., Dubreil, L., Gouin, S.G., Combal, J.P., et al. (2019). Chemical modification of the adeno-associated virus capsid to improve gene delivery. Chem. Sci. *11*, 1122–1131. https://doi.org/10.1039/c9sc04189c.

28. Schiroli, G., Conti, A., Ferrari, S., Della Volpe, L., Jacob, A., Albano, L., Beretta, S., Calabria, A., Vavassori, V., Gasparini, P., et al. (2019). Precise Gene Editing Preserves Hematopoietic Stem Cell Function following Transient p53-Mediated DNA Damage Response. Cell Stem Cell *24*, 551–565.e8. https://doi.org/10.1016/j.stem.2019.02.019.

29. Schambach, A., Buchholz, C.J., Torres-Ruiz, R., Cichutek, K., Morgan, M., Trapani, I., and Büning, H. (2024). A new age of precision gene therapy. Lancet *403*, 568–582. https://doi.org/10.1016/S0140-6736(23)01952-9.

30. Ozelo, M.C., Mahlangu, J., Pasi, K.J., Giermasz, A., Leavitt, A.D., Laffan, M., Symington, E., Quon, D.V., Wang, J.-D., Peerlinck, K., et al. (2022). Valoctocogene Roxaparvovec Gene Therapy for Hemophilia A. N. Engl. J. Med. *386*, 1013–1025. https://doi.org/10.1056/NEJMoa2113708.

31. Crudele, J.M., and Chamberlain, J.S. (2019). AAV-based gene therapies for the muscular dystrophies. Hum. Mol. Genet. *28*, R102–R107. https://doi.org/10.1093/hmg/ddz128.

32. Prado, D.A., Acosta-Acero, M., and Maldonado, R.S. (2020). Gene therapy beyond luxturna: a new horizon of the treatment for inherited retinal disease. Curr. Opin. Ophthalmol. *31*, 147–154. https://doi.org/10.1097/ICU.0000000000000660.

33. Lopez-Gordo, E., Chamberlain, K., Riyad, J.M., Kohlbrenner, E., and Weber, T. (2024). Natural Adeno-Associated Virus Serotypes and Engineered Adeno-Associated Virus Capsid Variants: Tropism Differences and Mechanistic Insights. Viruses *16*, 442. https://doi.org/10.3390/v16030442.

34. Veldwijk, M.R., Fruehauf, S., Schiedlmeier, B., Kleinschmidt, J.A., and Zeller, W.J. (2000). Differential expression of a recombinant adeno-associated virus 2 vector in human CD34+ cells and breast cancer cells. Cancer Gene Ther. *7*, 597–604. https://doi.org/10.1038/sj.cgt.7700159.

35. Santat, L., Paz, H., Wong, C., Li, L., Macer, J., Forman, S., Wong, K.K., and Chatterjee, S. (2005). Recombinant AAV2 transduction of primitive human hematopoietic stem cells capable of serial engraftment in immune-deficient mice. Proc. Natl. Acad. Sci. USA *102*, 11053–11058. https://doi.org/10.1073/pnas.0502902102.

36. Ferrari, S., Jacob, A., Beretta, S., Unali, G., Albano, L., Vavassori, V., Cittaro, D., Lazarevic, D., Brombin, C., Cugnata, F., et al. (2020). Efficient gene editing of human long-term hematopoietic stem cells validated by clonal tracking. Nat. Biotechnol. *38*, 1298–1308. https://doi.org/10.1038/s41587-020-0551-y.

37. Brault, J., Liu, T., Bello, E., Liu, S., Sweeney, C.L., Meis, R.J., Koontz, S., Corsino, C., Choi, U., Vayssiere, G., et al. (2021). CRISPR-targeted MAGT1 insertion restores XMEN patient hematopoietic stem cells and lymphocytes. Blood *138*, 2768–2780. https://doi.org/10.1182/blood.2021011192.

38. Haapaniemi, E., Botla, S., Persson, J., Schmierer, B., and Taipale, J. (2018). CRISPR-Cas9 genome editing induces a p53-mediated DNA damage response. Nat. Med. *24*, 927–930. https://doi.org/10.1038/s41591-018-0049-z.

39. Ferrari, S., Jacob, A., Cesana, D., Laugel, M., Beretta, S., Varesi, A., Unali, G., Conti, A., Canarutto, D., Albano, L., et al. (2022). Choice of template delivery mitigates the genotoxic risk and adverse impact of editing in human hematopoietic stem cells. Cell Stem Cell *29*, 1428–1444.e9. https://doi.org/10.1016/j.stem.2022.09.001.

40. Hendel, A., Fine, E.J., Bao, G., and Porteus, M.H. (2015). Quantifying on- and off-target genome editing. Trends Biotechnol. *33*, 132–140. https://doi.org/10.1016/j.tibtech.2014.12.001.

41. Cameron, P., Fuller, C.K., Donohoue, P.D., Jones, B.N., Thompson, M.S., Carter, M.M., Gradia, S., Vidal, B., Garner, E., Slorach, E.M., et al. (2017). Mapping the genomic landscape of CRISPR-Cas9 cleavage. Nat. Methods *14*, 600–606. https://doi.org/10.1038/nmeth.4284.

42. De Ravin, S.S., Li, L., Wu, X., Choi, U., Allen, C., Koontz, S., Lee, J., Theobald-Whiting, N., Chu, J., Garofalo, M., et al. (2017). CRISPR-Cas9 gene repair of hematopoietic stem cells from patients with X-linked chronic granulomatous disease. Sci. Transl. Med. *9*, eaah3480. https://doi.org/10.1126/scitranslmed.aah3480.

43. Charlesworth, C.T., Camarena, J., Cromer, M.K., Vaidyanathan, S., Bak, R.O., Carte, J.M., Potter, J., Dever, D.P., and Porteus, M.H. (2018). Priming Human Repopulating Hematopoietic Stem and Progenitor Cells for Cas9/sgRNA Gene Targeting. Mol. Ther. Nucleic Acids *12*, 89–104. https://doi.org/10.1016/j.omtn.2018.04.017.

44. Mani, M., Venkatasubrahmanyam, S., Sanyal, M., Levy, S., Butte, A., Weinberg, K., and Jahn, T. (2009). Wiskott-Aldrich syndrome protein is an effector of Kit signaling. Blood *114*, 2900–2908. https://doi.org/10.1182/blood-2009-01-200733.

45. Ferrua, F., Marangoni, F., Aiuti, A., and Roncarolo, M.G. (2020). Gene therapy for Wiskott-Aldrich syndrome: History, new vectors, future directions. J. Allergy Clin. Immunol. *146*, 262–265. https://doi.org/10.1016/j.jaci.2020.06.018.

46. Girard-Gagnepain, A., Amirache, F., Costa, C., Lévy, C., Frecha, C., Fusil, F., Nègre, D., Lavillette, D., Cosset, F.-L., and Verhoeyen, E. (2014). Baboon envelope pseudotyped LVs outperform VSV-G-LVs for gene transfer into early-cytokine-stimulated and resting HSCs. Blood *124*, 1221–1231. https://doi.org/10.1182/blood-2014-02-558163.

47. Maurice, M., Verhoeyen, E., Salmon, P., Trono, D., Russell, S.J., and Cosset, F.-L. (2002). Efficient gene transfer into human primary blood lymphocytes by surface-engineered lentiviral vectors that display a T cell–activating polypeptide. Blood *99*, 2342–2350. https://doi.org/10.1182/blood.V99.7.2342.

48. Lock, M., McGorray, S., Auricchio, A., Ayuso, E., Beecham, E.J., Blouin-Tavel, V., Bosch, F., Bose, M., Byrne, B.J., Caton, T., et al. (2010). Characterization of a recombinant adeno-associated virus type 2 Reference Standard Material. Hum. Gene Ther. *21*, 1273–1285. https://doi.org/10.1089/hum.2009.223.

49. D'Costa, S., Blouin, V., Broucque, F., Penaud-Budloo, M., François, A., Perez, I.C., Le Bec, C., Moullier, P., Snyder, R.O., and Ayuso, E. (2016). Practical utilization of recombinant AAV vector reference standards: focus on vector genomes titration by free ITR qPCR. Mol. Ther. Methods Clin. Dev. *5*, 16019. https://doi.org/10.1038/mtm.2016.19.

50. Lévy, C., Amirache, F., Girard-Gagnepain, A., Frecha, C., Roman-Rodríguez, F.J., Bernadin, O., Costa, C., Nègre, D., Gutierrez-Guerrero, A., Vranckx, L.S., et al. (2017). Measles virus envelope pseudotyped lentiviral vectors transduce quiescent human HSCs at an efficiency without precedent. Blood Adv. *1*, 2088–2104. https://doi.org/10.1182/bloodadvances.2017007773.